





Effects of infection fatality ratio and social contact matrices on vaccine prioritization strategies

Arthur Schulenburg ¹, Wesley Cota ^{1, a)}, Guilherme S. Costa ¹ and Silvio C. Ferreira ^{1, 2}

¹⁾Departamento de Física, Universidade Federal de Viçosa, Viçosa, Minas Gerais, 36570-900 Brazil

²⁾National Institute of Science and Technology for Complex Systems, Rio de Janeiro, 22290-180 Brazil

(*Electronic mail: silviojr@ufv.br)

(*Electronic mail: wesley@wcota.me)

(Dated: 9 August 2022)

Effective strategies of vaccine prioritization are essential to mitigate the impacts of severe infectious diseases. We investigate the role of infection fatality ratio (IFR) and social contact matrices on vaccination prioritization using a compartmental epidemic model fueled by real-world data of different diseases and countries. Our study confirms that massive and early vaccination is extremely effective to reduce the disease fatality if the contagion is mitigated, but the effectiveness is increasingly reduced as vaccination beginning delays in an uncontrolled epidemiological scenario. The optimal and least effective prioritization strategies depend non-linearly on epidemiological variables. Regions of the epidemiological parameter space, in which prioritizing the most vulnerable population is more effective than the most contagious individuals, depend strongly on the IFR age profile being, for example, substantially broader for COVID-19 in comparison with seasonal influenza. Demographics and social contact matrices deform the phase diagrams but do not alter their qualitative shapes.

Accepted in Chaos: An Interdisciplinary Journal of Nonlinear Science

Modeling of epidemic diseases allows the evaluation of possible strategies and their impacts in mitigating the threat of emerging infectious diseases. We investigate a mathematical model to discern the most effective vaccination strategies to reduce the fatality of infectious diseases. The method uses data from different countries (Brazil, Germany, and Uganda), social life scenarios (adopting or not social distancing), and other epidemiological parameters to fuel the computational simulations to analyze the most effective prioritization scheme. We report not only that early and massive vaccination is important, but also vaccinating first the most vulnerable individuals is the most effective to reduce deaths due to the disease in highly infectious scenarios while prioritizing the most exposed population, who make more social contacts, can be more effective in reducing the number of deaths when the disease is spreading slowly. Determination of the most effective strategy is a multifactorial process that depends on disease specifics, such as the age profile of the disease fatality and vaccination efficacy, and non-biological features such as vaccination distribution, social contacts, and demographics.

I. INTRODUCTION

Densely connected and unequal societies impose enormous challenges for combating emerging infectious diseases and

their potentially catastrophic consequences. The ongoing COVID-19 pandemic is an example that has reshaped the form of how people interact. Several and variable nonpharmacological interventions (NPIs) can be adopted across different places, as wearing of face masks, physical and social distancing, as well as more extreme ones such as lockdown, school closure, and traveling restrictions¹⁻⁵. While being clearly efficient to momentarily reduce the transmission and unburden health systems^{4,5}, they are insufficient to restore the pre-pandemic lifestyle and avoid economic crashes caused by the disease⁶. Natural emergence of virus variants⁷⁻¹³, fueled by negligent human behaviors, means that natural herd immunity by infections, in which individuals are immune and the susceptible pool is insufficient to a sustained transmission¹⁴, is hard to be achieved¹⁵.

We have recently witnessed the development of vaccines for COVID-19 with unprecedented speed due to immense collaborative efforts, resources, and accumulated expertise from other viral infectious diseases^{16,17}. All vaccines approved for emergency use had a high potential to prevent severe cases after complete vaccination and immunization whose time depends on the type of vaccine. However, as usual for anti-viral vaccines, the capacity of COVID-19 vaccines to impede infections and mild symptoms is lower than their efficiency to reduce death and severe cases¹⁸⁻²². Indeed, while herd immunity is an important aim of massive vaccination, its main emergency function is to prevent severe cases which can result in deaths and serious sequelae²³⁻²⁷.

The development of efficient vaccines is only the first challenge preceding massive immunization. Large-scale production and timely distribution, particularly to low-income economies, remain a major barrier to drastically reduce severe cases and to reach herd immunity²⁸⁻³⁰. Another great matter of concern, especially for high-income economies, is the low

^{a)}Also at Instituto de Medicina Tropical, Universidade de São Paulo, São Paulo, 05403-000 Brazil & Departamento de Infectologia, Faculdade de Medicina de Botucatu, Universidade Estadual Paulista, Botucatu, São Paulo, 18618-687 Brazil

demand for vaccines by the population, which not rarely refuses to get their shots or to complete the immunization schedule. Therefore, given the finite capacity of vaccination, the logistic must be engineered to minimize damages^{23,24,26,27,31–36}. Infection fatality ratio (IFR) is age- and illness-dependent due to, among other factors, cumulative comorbidities^{37–43}. While on the one hand, infectious diseases, and particularly COVID-19, present very high IFR on elderly in contrast with much lower values among kids and newborns^{42–45}, on the other hand, younger population are socially more active and exposed to infections, being potentially the key vectors for contagion of the most vulnerable population^{46–48}. Finally, but not least, the level of sustained transmission is also decisive for the degree of success in vaccination campaigns^{30,33–35,48,49}.

In the present work, we investigate the role of vaccination on an age-structured compartmental model¹⁴, following a susceptible-exposed-asymptomatic-infected-recovered-deceased (SEAIRD) dynamics in different hypothetical scenarios, using social contact matrices⁵⁰ obtained for countries with very distinct population age distribution, namely Brazil, Germany, and Uganda. The approach then consists fundamentally of coupling data on human behavior with epidemic and vaccination dynamics⁵¹. Outcomes for age-dependent IFR estimated for COVID-19^{42–44} are compared with seasonal influenza⁴⁵. The interplay between vaccine efficacy to prevent deaths after complete immunization and the time taken to acquire protection were also addressed. Epidemic scenarios representing different levels of NPIs were studied. We have found that massive vaccination, even with modest protection against infections, is effective to reduce the disease fatality if adopted early and concomitantly with contagion mitigation, but loses effectiveness as the epidemic transmission becomes uncontrolled. Comparing different prioritization strategies, vaccinating the most vulnerable individuals first is the optimal strategy to reduce deaths for high transmission scenarios while distributing first shots to the most exposed ones can be better in lower transmission regimes. The region of the epidemiological parameters' space, in which prioritization of the vulnerable population is the most effective strategy, depends on the IFR and, thus, is disease dependent. Demographics quantitatively change the phase diagrams of the optimal strategy but preserve their qualitative aspects. Finally, we also analyzed the least effective strategies in a pool of four proposals and found out a dependence on epidemiological parameters more complex than the case of the optimal strategy, in which the phase diagrams indicating the least effective strategy depends strongly on both IFR and demographics. This is a result of the feedback loop between the disease dynamics and vaccination⁵¹, that must be taken into account by health authorities.

The remaining of the paper is organized as follows. We describe the model and parameters used in the data-driven approach in section II. Results dealing with four prioritization strategies are shown in section III. We conclude the paper discussing the main results in section IV.

II. MODELING THE DISEASE DYNAMICS

A. SEAIRD compartmental model and contact matrices

We start by considering a SEAIRD, age-structured, compartmental model¹⁴ to simulate the epidemic spreading without vaccination. The schematic representation of this dynamics is shown in Fig. 1. Individuals can belong to the following overall compartments: S (susceptible), E (exposed), A (asymptomatic or presymptomatic), I (infected), R (recovered), and D (deceased). Every compartment is subdivided according to the age group $i = 1, \dots, N_g$. Susceptible individuals of age group i become exposed with rate $\Pi^{(i)}$ upon contact with infectious individuals (labeled by \star in Fig. 1) of all age groups according to the contact matrix to be defined below. The other transitions are spontaneous: $E \rightarrow A$ happens with rate $\mu_A^{(i)}$; $A \rightarrow I$ and $A \rightarrow R$ have rates $\beta_I^{(i)}$ and $\beta_R^{(i)}$, respectively; those in the compartment I recover from the disease or die with rates $\alpha_R^{(i)}$ or $\alpha_D^{(i)}$, respectively. Recovered individuals are assumed to be permanently immunized but still demand vaccines.

We consider individuals divided into $N_g = 16$ age groups, starting from 0–4, 5–9, up to 70–74 and ≥ 75 years, and denote $n^{(i)}$ as the number of individuals in age group $i = 1, \dots, 16$. We refer to *young* population as those with age 0 to 19, *adults* for 20 to 59, and *elderly* with age equal or above 60 years. The relative size of each group is given in Table I for three countries investigated in the present work. The estimates for the Brazilian demographics of 2020⁵² are shown in Fig. 2(a).

TABLE I. Distribution of the population of young, adult, and elderly individuals in Brazil⁵², Germany⁵³, and Uganda⁵³.

	young	adult	elderly
Brazil	27.9%	57.6%	14.5%
Germany	18.9%	52.0%	29.1%
Uganda	57.1%	39.6%	3.3%

The infection rate of a susceptible individual within a group i is given by

$$\Pi^{(i)} = \frac{k_i}{n} \sum_j C_{ij} \left(\lambda_A A^{(j)} + \lambda_I I^{(j)} + \lambda_{A_V} A_V^{(j)} + \lambda_{I_V} I_V^{(j)} + \lambda_{I_P} I_P^{(j)} \right), \quad (1)$$

where the corresponding number of individuals in each compartment $\mathcal{Z} \in \{A, I, A_V, I_V, I_P\}$ and age group i is denoted by the italicized symbols (*e.g.* $I^{(i)}$ is the number of infected individuals belonging to age group i), while the corresponding infection rate per contact is represented by $\lambda_{\mathcal{Z}}$. In Eq. (1), k_i is the number of contacts made by an individual of age group i , C_{ij} is the fraction of contacts per individual of age group i with those of group j , and n is the total population.

To construct the contact matrices for C_{ij} and k_i we extracted the estimated number of contacts made by individuals of age

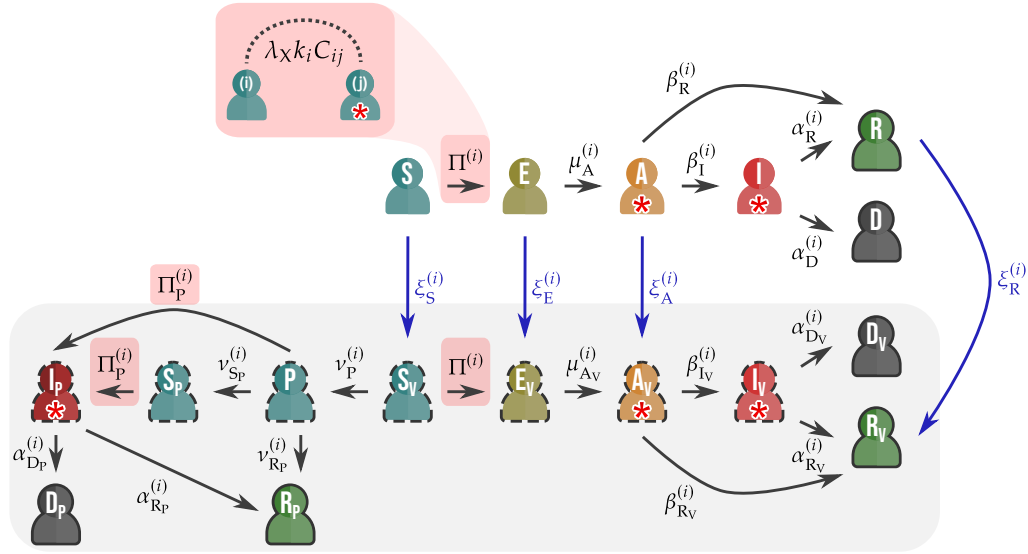


FIG. 1. Schematic representation of an age-structured compartmental model for epidemic dynamics with vaccination. The transitions between compartments (labels are defined in the main text) and the corresponding rates (see Table II and Eq. (1)) are indicated by arrows. The \star symbol refers to the infectious individuals. The catalytic transitions highlighted in the top represent the contagions of susceptible individuals, vaccinated or not, upon infectious contacts, while the remaining transitions are spontaneous.

groups i and j , denoted by m_{ij} , from data for three countries (Brazil, Uganda, and Germany) and 16 age groups (0–4, 5–9, \dots , 75–79) reported in Ref.⁵⁰. We assume that individuals with age ≥ 80 follow the same contact patterns of those in group 75–79, considering a single age group ≥ 75 . Reference⁵⁰ reports matrices for contacts made at home, work, school, and other places in a situation without epidemic mitigation. The mitigation scenarios are modeled by the reduction of contacts in specific places. The values of $m_{ij}^{\{X\}}$ for a mitigation scenario $\{X\}$ are given by an weighted sum of the original matrices considering the fraction of contacts allowed in each place. It is important to ensure that the number of contacts among individuals of different groups are symmetric defining another contact matrix with values c_{ij} where the total number of contacts made by individuals from age group i with j , $n^{(i)}c_{ij}$, is the same as those of j with i , $n^{(j)}c_{ji}$. This is possible using⁵⁴

$$c_{ij} = \frac{m_{ij}n^{(i)} + m_{ji}n^{(j)}}{2n^{(i)}}, \quad (2)$$

in which $i, j = 1, \dots, 16$ and obeys the balance condition $n^{(i)}c_{ij} = n^{(j)}c_{ji}$. The average number of contacts made by individuals in age group i is defined as

$$k_i = \sum_j c_{ij}. \quad (3)$$

Finally, the normalized contact matrix elements C_{ij} are given by the relation $c_{ij} = k_i C_{ij}$ and used in Eq. (1).

We emulate a hypothetical epidemic scenario of *social distancing*, denoted by $\{S\}$, where 100%, 50%, 50%, and 30% of contacts are allowed in home, work, school, and other places, respectively. The social distancing will be compared with the

unmitigated scenario, denoted by $\{U\}$, where no reduction of contacts is implemented. The respective average number of contacts in different age groups for Brazil considering each scenario is shown in Fig. 2(a). Adopting the symmetrization procedure described before, we compute the contact matrices of Brazil shown in Fig. 2(b). For instance, the average number of contact decays from $\langle k \rangle \approx 15$ in the unmitigated scenario to 8.3 when the social distancing is adopted. Equivalent figures for Uganda and Germany are provided in Section SI-I of the SM⁵⁵.

To simulate the epidemic dynamics we consider a set of ordinary differential equations considering the transition rates and compartments schematically given in Fig. 1. The evolution of the compartments of unvaccinated individuals is given by the following set of equations:

$$\frac{dS^{(i)}}{dt} = -\Pi^{(i)}S^{(i)} - \xi_S^{(i)}S^{(i)}, \quad (4a)$$

$$\frac{dE^{(i)}}{dt} = \Pi^{(i)}S^{(i)} - \left(\xi_E^{(i)} + \mu_A^{(i)} \right) E^{(i)}, \quad (4b)$$

$$\frac{dA^{(i)}}{dt} = \mu_A^{(i)}E^{(i)} - \left(\xi_A^{(i)} + \beta_I^{(i)} + \beta_R^{(i)} \right) A^{(i)}, \quad (4c)$$

$$\frac{dI^{(i)}}{dt} = \beta_I^{(i)}A^{(i)} - \left(\alpha_R^{(i)} + \alpha_D^{(i)} \right) I^{(i)}, \quad (4d)$$

$$\frac{dR^{(i)}}{dt} = \beta_R^{(i)}A^{(i)} + \alpha_R^{(i)}I^{(i)} - \xi_R^{(i)}R^{(i)}, \quad (4e)$$

$$\frac{dD^{(i)}}{dt} = \alpha_D^{(i)}I^{(i)}, \quad (4f)$$

in which $\Pi^{(i)}$ is given by Eq. (1) and the italicized capital letters represent the number of individuals of age group i in the compartment labeled with the same symbol.

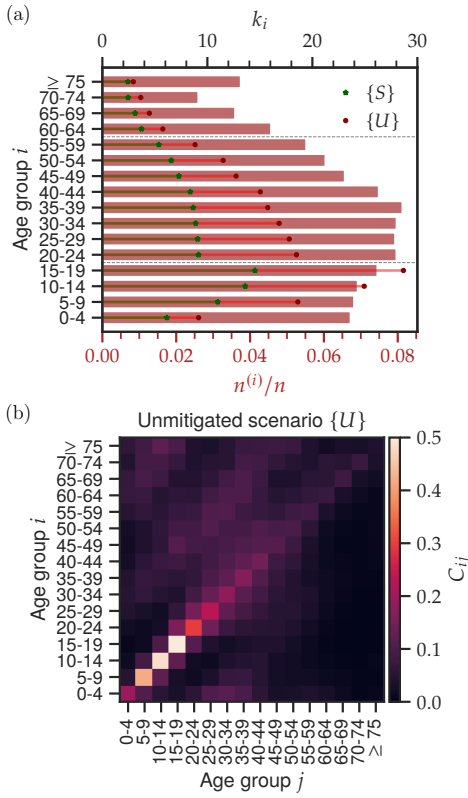


FIG. 2. Demographic and contact patterns in Brazil considered in the age-structured compartmental model. (a) Fraction of individuals $n^{(i)}/n$ for each age group i (bars) and their mean number of contacts k_i (symbols) for social distancing $\{S\}$ and unmitigated $\{U\}$ scenarios. Solid lines represent the increase from one scenario to the other and dashed lines divide the age groups into young, adult and elderly individuals. (b) Contact matrix C_{ij} in the unmitigated scenario of Brazil. Data adapted from Refs.^{50,52} as described in the main text.

The basic reproduction number¹⁴ R_0 in absence of vaccines is given by the sum of the contributions from every infectious compartment, which are A and I individuals in the present work. The contribution from asymptomatic infections is given by

$$R_0^A = \sum_{ij} \frac{S^{(i)}}{n} a_j k_i C_{ij} \frac{\lambda_A}{\beta_I^{(i)} + \beta_R^{(i)}}, \quad (5)$$

where $n = \sum_i n^{(i)}$ and a_j is the probability that an infected individual is introduced in age group j in a totally susceptible population, which is assumed to be proportional to the total number of contacts made by group j and given by¹⁴

$$a_j = \frac{k_j n^{(j)}}{\sum_l k_l n^{(l)}} = \frac{k_j n^{(j)}}{n \langle k \rangle}. \quad (6)$$

Here, $\langle k \rangle = \sum_i k_i n^{(i)}/n$ is the average number of contacts. The infection rate λ_A per contact is assumed to be the same for all age groups while the mean time for which the individual of age group i remains asymptomatic is given by

$1/(\beta_I^{(i)} + \beta_R^{(i)})$. The final expression for R_0^A becomes

$$R_0^A = \sum_{ij} \frac{\lambda_A n^{(i)} n^{(j)} k_i k_j C_{ij}}{n^2 \langle k \rangle (\beta_I^{(i)} + \beta_R^{(i)})}. \quad (7)$$

For the infected compartment, we consider the probability that the introduced individual becomes symptomatic, $\beta_I^{(i)}/(\beta_I^{(i)} + \beta_R^{(i)})$, and the mean time that they remain infectious, $1/(\alpha_D^{(i)} + \alpha_R^{(i)})$, and a similar calculation leads to

$$R_0^I = \sum_{ij} \frac{\lambda_I}{\alpha_D^{(i)} + \alpha_R^{(i)}} \frac{n^{(i)} n^{(j)} k_i k_j C_{ij} \beta_I^{(i)}}{n^2 \langle k \rangle (\beta_I^{(i)} + \beta_R^{(i)})}. \quad (8)$$

Summing both contributions, we have:

$$R_0 = \sum_{i,j=1}^{N_g} \frac{n^{(i)} n^{(j)} k_i k_j C_{ij}}{n^2 \langle k \rangle (\beta_I^{(i)} + \beta_R^{(i)})} \left[\lambda_A + \frac{\lambda_I \beta_I^{(i)}}{\alpha_D^{(i)} + \alpha_R^{(i)}} \right]. \quad (9)$$

Infection rate λ , assumed as $\lambda_{\mathcal{Z}} = \lambda$ for $\mathcal{Z} \in \{A, I, A_V, I_V\}$ and $\lambda_{I_p} = \lambda/2$, is parameterized as a function of a control parameter ω using Eq. (9) such that $\omega \equiv R_0^{\{S\}}$ for the case of social distancing scenario. The parameter ω is easier to interpret than λ since it quantifies the level of the epidemic spreading in terms of a dimensionless quantity. In the interval $\omega \in [1, 2]$, the basic reproduction number of the unmitigated scenario is compatible with the SARS-CoV-2 ranges $R_0 \in [2, 4]$ estimated at the beginning of the COVID-19 pandemics^{56–59}. The computation of these values for both unmitigated and social distancing scenarios as a function of a parameter $\omega = R_0^{\{S\}}$, defined for a social distancing scenario, is shown in Fig. 3. The interval $\omega \in [1, 2]$ allows to mimic different levels of NPIs.

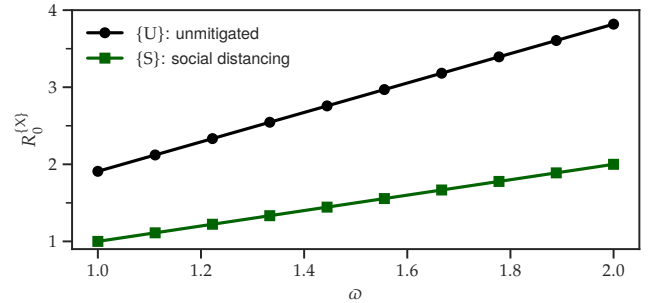


FIG. 3. Parameterization of the basic reproduction number $R_0^{\{X\}}$ considering two different contact scenarios. The value of $R_0^{\{X\}}$ is computed using Eq. (9) for each scenario $\{X\}$ (indicated in the legend) as function of the parameter ω for Brazil.

B. Age-dependent infection fatality ratio

The infection fatality ratio (IFR) considers all infections including the asymptomatic and paucisymptomatic ones, which

may not be documented⁴⁴, differently of the case fatality ratio, which is the fraction of confirmed cases that evolve to death. We define the IFR as the fraction $\Theta^{(i)}$ of infected individuals that evolve to death, and can be straightforwardly computed in terms of the model's rates (Fig. 1) as

$$\Theta^{(i)} = \frac{\beta_I^{(i)} \alpha_D^{(i)}}{\beta_I^{(i)} + \beta_R^{(i)} \alpha_R^{(i)} + \alpha_D^{(i)}}, \quad (10)$$

which can be inverted to determine the rate $\alpha_D^{(i)}$ in terms of the IFR and other experimentally determined epidemiological parameters and then $\alpha_D^{(i)}$ is used in the simulation of the model equations; See Table II. Here we used the IFR estimates for COVID-19 reported by Verity *et al.*⁴⁴, that follows an exponential increase with age. Similar values have been reported elsewhere^{42,43}. To investigate the role of IFR, data for influenza from the *Centers for Disease Control and Prevention*⁴⁵ and a hypothetical uniform IFR, given by the averaged COVID-19's IFR weighted by the population size of each age group, were also considered while the remaining parameters were the same estimated for COVID-19. Influenza's IFR also increases exponentially with age, but it is lower than for COVID-19 and influences the choice of the vaccination strategies^{24,33}. The IFR age dependence is shown in Fig. 4.

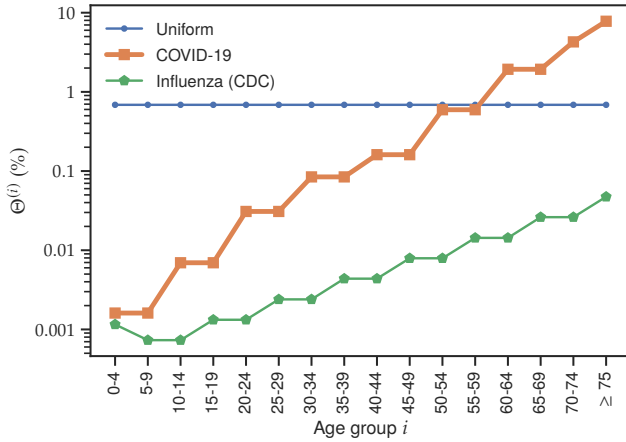


FIG. 4. Age-dependent infection fatality ratio (IFR) for two different diseases and a baseline value. The IFR $\Theta^{(i)}$ for each age group i is shown for COVID-19⁴²⁻⁴⁴, influenza⁴⁵, and a uniform value of 0.68% considered as a baseline, given by the average for COVID-19's IFR weighted by the population of each age group.

C. Vaccination dynamics and strategies

Individuals of compartments $Z \in \{S, E, A, R\}$ can receive a vaccine shot and move to the corresponding vaccinated compartments $\mathcal{Z}_V \in \{S_V, E_V, A_V, R_V\}$ with the respective rates $\xi_{\mathcal{Z}}^{(i)}$; See Eq. (15). The transmission dynamics of vaccinated individuals belonging to \mathcal{Z}_V are the same as \mathcal{Z} with their respective transition rates. Additionally, those in the S_V compartment can turn into P with rate $v_P^{(i)}$, conferring protection

against death with high probability. The inverse of this rate is associated with the time between vaccine shots, an important epidemiological parameter. The protected individuals P can evolve to either susceptible S_P or directly to recovered R_P states with rates $v_{S_P}^{(i)}$ and $v_{R_P}^{(i)}$, depending on the vaccine efficacy against infections $\psi_{\text{inf}}^{(i)}$, respectively: S_P individuals can still be infected, transmit the pathogen, and eventually die, whereas R_P individuals are fully protected against both infection and death. The probability that a protected individual acquires full protection, given by

$$\psi_{\text{inf}}^{(i)} = \frac{v_{R_P}^{(i)}}{v_{R_P}^{(i)} + v_{S_P}^{(i)}}, \quad (11)$$

is directly obtained from the model and used to parameterize the rates in terms of the vaccine efficacy against infection and a characteristic time $1/(v_{R_P}^{(i)} + v_{S_P}^{(i)})$. Both P and S_P individuals can be infected with rate $\Pi_P^{(i)}$ which is explained below. For the sake of simplicity, the infections of protected individuals follow a SIR-like dynamics with a single infectious compartment I_P which can be recovered (move to R_P) or die (move to D_P) with rates $\alpha_{R_P}^{(i)}$ or $\alpha_{D_P}^{(i)}$, respectively. The last two rates can also be parameterized in terms of the efficacy to prevent deaths which is the reduction of the probability that an infected protected individual dies in comparison with an unprotected population. It can be calculated in terms of the model rates resulting in the following relation

$$(1 - \psi_{\text{death}}^{(i)}) \Theta^{(i)} = \frac{\alpha_{D_P}^{(i)}}{\alpha_{R_P}^{(i)} + \alpha_{D_P}^{(i)}}, \quad (12)$$

in which $\Theta^{(i)}$ is the IFR of group age i . Using the experimentally determined epidemiological parameters, IFR, and efficacy against death we then determine $\alpha_{D_P}^{(i)}$ from Eq. (12); See Table II.

For sake of simplicity, individuals are labeled as vaccinated after the first shot, but acquire protection and are moved to the compartment $P^{(i)}$ only after the second shot. The average interval between shots, which corresponds to the transition $S_V \rightarrow P$ is given by $1/v_{S_P}^{(i)}$, assumed uniform across age groups. With respect to the efficacy against infection and death, both an ideal case with moderate protection ($\psi_{\text{inf}}^{(i)} = 50\% \forall i$) against infection with full protection against death ($\alpha_{D_P}^{(i)} = 0 \forall i$), and an age-dependent efficacy based in the values reported in Ref.⁶⁰, for which elderly individuals have reduced protection, are simulated. We considered data for CoronaVac effectiveness against infection and death for individuals who received two shots, based on values reported in Ref.⁶⁰, which are available for age groups < 60, 60–69, 70–79, 80–89 and ≥ 90 years old. We assume a constant efficacy against infection for individuals with < 75 years, and constant efficacy against death for < 70 years. The reported value for 70–79 is used as the efficacy against death for the age group 70–74, while an average weighted by the populations is used to obtain the values for individuals of ≥ 75

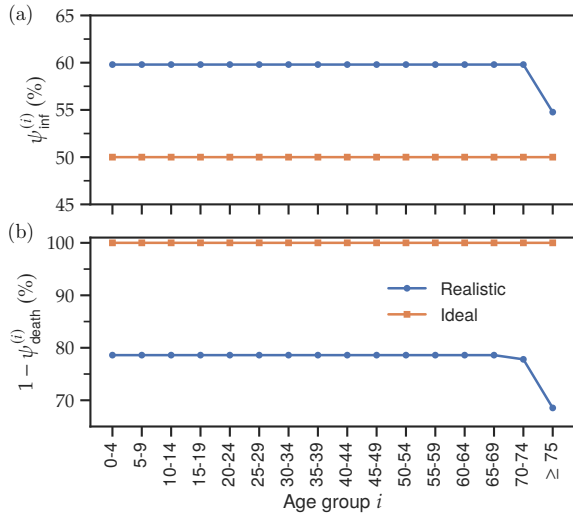


FIG. 5. Age-dependent vaccine efficacy against infection and death for realistic and ideal vaccines. The values of protection (a) against infection, ψ_{inf} , and (b) against death, $1 - \psi_{\text{death}}$, are given for the realistic and ideal vaccine models. The realistic values are based in Ref.⁶⁰ and details are given in the main text.

years in both cases. Realistic and ideal models for protection are shown in Fig. 5. In all cases, after an average time of $1/(v_{R_P} + v_{S_P}) = 7$ days, uniform across ages, they either become fully immunized ($P \rightarrow R_P$) or remain susceptible to the disease ($P \rightarrow S_P$).

The dynamics of vaccinated individuals is highlighted in the shaded area of Fig. 1 and the temporal evolution of the vaccinated compartments is given by the following set of equations:

$$\frac{dS_V^{(i)}}{dt} = -(\Pi^{(i)} + v_P^{(i)})S_V^{(i)} + \xi_S^{(i)}S^{(i)}, \quad (13a)$$

$$\frac{dE_V^{(i)}}{dt} = \Pi^{(i)}S_V^{(i)} + \xi_E^{(i)}E^{(i)} - \mu_{A_V}^{(i)}E_V^{(i)}, \quad (13b)$$

$$\frac{dA_V^{(i)}}{dt} = \mu_{A_V}^{(i)}E_V^{(i)} + \xi_A^{(i)}A^{(i)} - (\beta_{I_V}^{(i)} + \beta_{R_V}^{(i)})A_V^{(i)}, \quad (13c)$$

$$\frac{dI_V^{(i)}}{dt} = \beta_{I_V}^{(i)}A_V^{(i)} - (\alpha_{R_V}^{(i)} + \alpha_{D_V}^{(i)})I_V^{(i)}, \quad (13d)$$

$$\frac{dR_V^{(i)}}{dt} = \alpha_{R_V}^{(i)}I_V^{(i)} + \beta_{R_V}^{(i)}A_V^{(i)} + \xi_R^{(i)}R^{(i)}, \quad (13e)$$

$$\frac{dD_V^{(i)}}{dt} = \alpha_{D_V}^{(i)}I_V^{(i)}. \quad (13f)$$

Finally, individuals that develop immune response to the disease are protected and can turn into P , S_P , I_P , R_P , and D_P compartments, which evolve as

$$\frac{dP^{(i)}}{dt} = v_P^{(i)}S_V^{(i)} - (\Pi_P^{(i)} + v_{S_P}^{(i)} + v_{R_P}^{(i)})P^{(i)}, \quad (14a)$$

$$\frac{dS_P^{(i)}}{dt} = v_{S_P}^{(i)}P^{(i)} - \Pi_P^{(i)}S_P^{(i)}, \quad (14b)$$

$$\frac{dI_P^{(i)}}{dt} = \Pi_P^{(i)}P^{(i)} + \Pi_P^{(i)}S_P^{(i)} - (\alpha_{R_P}^{(i)} + \alpha_{D_P}^{(i)})I_P^{(i)}, \quad (14c)$$

$$\frac{dR_P^{(i)}}{dt} = v_{R_P}^{(i)}P^{(i)} + \alpha_{R_P}^{(i)}I_P^{(i)}, \quad (14d)$$

$$\frac{dD_P^{(i)}}{dt} = \alpha_{D_P}^{(i)}I_P^{(i)}. \quad (14e)$$

For sake of simplicity, we consider the same infection rate for protected and non-vaccinated susceptible individuals, $\Pi_P^{(i)} = \Pi^{(i)}$, assuming the former is less contagious ($\lambda_{I_P} < \lambda_{\mathcal{I}}$) due to a reduced viral load⁶¹.

The rate $\xi(t)$ is defined as the per capita number of daily first shots of vaccines. For sake of generality, it is assumed to be time-dependent even though we performed simulations assuming ξ constant in the present work. Let us define $\Omega^{(i)}(t) = 1$ if age group i is being vaccinated at time t and $\Omega^{(i)}(t) = 0$ otherwise. All non-vaccinated individuals belonging to the compartments $S^{(i)}$, $E^{(i)}$, $A^{(i)}$, or $R^{(i)}$ can receive their first shots with equal chance if they are scheduled, *i.e.*, if $\Omega^{(i)}(t) = 1$. Therefore, the vaccination rates of the compartments $\mathcal{I} \in \{S, E, A, R\}$ in age group i are given by

$$\xi_{\mathcal{I}}^{(i)}(t) = \frac{n\xi\Omega^{(i)}}{\sum_j [S^{(j)} + E^{(j)} + A^{(j)} + R^{(j)}] \Omega^{(j)}}. \quad (15)$$

For example, $\xi_S^{(i)}(t)$ is the vaccination rate of susceptible individuals of age group i .

The prioritization of vaccine shots across different age groups over time can be modeled with $\Omega^{(i)}(t)$. The vaccination begins at a time t_v such that $\Omega^{(i)}(t < t_v) = 0 \forall i$. Once 80% of a priority group has been vaccinated, the vaccination of the next priority groups starts concomitantly with all other groups where vaccination had started previously. Four prioritization strategies are investigated in the present work. In *decreasing age priority* (DAP) strategy, one starts in the oldest age group and proceeds progressively down to the youngest one as adopted in many countries for the general population. In *highly-vulnerable priority* (HVP) strategy, only the elderly are prioritized according to the age, then all adults (age 20–59) and later all young individuals (0–19) are vaccinated without age prioritization. This could represent the economically active population being vaccinated altogether after the most vulnerable individuals were protected. The *decreasing contact priority* (DCP) strategy starts with the age group of the higher number of contacts and proceeds progressively down to the one less connected. This strategy corresponds to vaccinating the most exposed first. Finally, in the *no priority* (NP) strategy all age groups are vaccinated concomitantly.

Finally, we integrate the dynamical system using initial conditions where a single exposed individual is introduced in a single age group s in a total population $n = 10^5$ individuals (results are insensitive to this parameter given it is large enough). The averages were computed over initial conditions $s = 1, \dots, N_g$ using as weight the total number of contacts made by each group s , in which the epidemic process is initiated. Table II presents all other epidemiological parameters used in the model or their respective relations.

TABLE II. Epidemiological parameters and rates used in the model.

Parameters	Description	Value	References
$\lambda_{\mathcal{Z}}, —$	Transmission rates for $\mathcal{Z} = A, I, A_V,$ and I_V	See Eq. (9)	—
$—, \lambda_{I_p}$	Transmission rate for partially protected individuals	$\frac{\lambda_{\mathcal{Z}}}{2}$	61
$\mu_A^{(i)}, \mu_{A_V}^{(i)}$	Latent period rate	$(5.2 \text{ days})^{-1}$	56
$\beta_I^{(i)}, \beta_{I_V}^{(i)}$	Asymptomatic period rate	$(2.6 \text{ days})^{-1}$	56
$\alpha_R^{(i)}, \alpha_{R_V}^{(i)}$	Recovering rate (with symptoms)	$(3.2 \text{ days})^{-1}$	62,63
$\beta_R^{(i)}, \beta_{R_V}^{(i)}$	Recovering rate (without symptoms)	$\frac{1}{\beta_I^{-1} + \alpha_R^{-1}}$	—
$\alpha_D^{(i)}, \alpha_{D_V}^{(i)}$	Death rate	See Eq. (10)	—
$—, v_p^{(i)}$	Immune response period rate	$(21 \text{ days})^{-1}$	64,65
$—, v_{R_p}^{(i)}$	Vaccine success rate	$\frac{1}{7 \text{ days}} \psi_{\text{inf}}^{(i)}$	—
$—, v_{S_p}^{(i)}$	Vaccine failing rate	$\frac{1}{7 \text{ days}} (1 - \psi_{\text{inf}}^{(i)})$	—
$—, \alpha_{R_p}^{(i)}$	Recovering rate for protected individuals	$\beta_R^{(i)}$	—
$—, \alpha_{D_p}^{(i)}$	Death rate for protected individuals	See Eq. (12)	—
$\xi_{\mathcal{Z}}^{(i)}, —$	Vaccination rate for a given compartment \mathcal{Z}	See Eq. (15)	—
$\Theta^{(i)}$	Infection fatality ratio	See Fig. 4	44,45
$\psi_{\text{inf}}^{(i)}$	Vaccine efficacy against infection	See Fig. 5	60
$\psi_{\text{death}}^{(i)}$	Vaccine efficacy against death	See Fig. 5	60

III. RESULTS AND DISCUSSION

A. DAP vaccination

Considering $\omega = 1.3$, social distancing scenario, modest vaccination with constant rate $\xi = 0.15\%$ of the population per day, age-dependent efficacy, short delay $t_v = 30$ days, and DAP vaccination strategy, we computed the fractions ρ_{inf} of infectious ($I, I_V, A, A_V,$ and I_p) and ρ_d of deceased ($D, D_V,$ and D_p) individuals to compare with the case without vaccines. Figures 6(a,b,d,e) present the temporal evolution of ρ_{inf} and ρ_d in the form of stack plots split according to the age profiles of young, adult, and elderly populations of Brazil. Even a modest vaccination rate, if started early, substantially reduces the total amount of deaths while the reduction of infections is not expressive. The age profiles for infections and deaths are shown in Figs. 6(c,f). Since the percentages of young, adults, and elderly in the Brazilian populations are 27.9%, 57.6%, and 14.5%⁵², respectively, the age profile of infections without vaccines is highly correlated with the demography, Fig. 6(c), while the deaths' profile is determined by the COVID-19's IFR used in these simulations: Figs. 4 and 6(f) show that deaths are highly concentrated in elderly, even they corresponding to the minor part of the population.

The DAP strategy moderately alters the age profile of infected individuals. Beyond reducing deaths in all age groups, the fatality age profile is highly affected, presenting a big drop in death among the elderly and a fractional rise in the adult population that now concentrates most of the deaths. Not sur-

prisingly, this inversion was observed during the first semester of 2021 in Brazil that adopted DAP after vaccination of healthcare workers and persons with morbid conditions. Remark that the age profile of deaths changes substantially after the lifespan of immune response $1/v_p^{(i)} = (21 \text{ days})^{-1}$, highlighting the importance of a complete immunization scheme. Similar results are found using uniform values of efficacy against death and infection, as shown in Section SI-II of the SM⁵⁵, with quantitative changes on the age profile due to the reduction of the drop of efficacy in the elderly individuals.

The interplay between vaccination rate ξ and effective infection rate parameterized by ω is investigated considering the DAP strategy and age-dependent values of efficacy with a delay of $t_v = 30$ days to start vaccination. Heatmaps for the reduction of deaths in the space parameter ξ versus ω under unmitigated and social distance contact scenarios are presented in Fig. 7 for Brazil contact matrices. The corresponding heatmaps for total recovered population is given in Fig. SI-4 of the SM⁵⁵. As expected, the reduction of deaths is much more expressive than of infections for both scenarios. In the scenario of social distancing shown in Fig. 7(a), DAP vaccination performs very well to reduce deaths if the immunization rate is not too low and dissemination rate is not too high (reduced ω); the latter is feasible through simple NPIs. For the case of unmitigated contacts shown in Fig. 7(b), the vaccination can significantly reduce the number of deaths only at a high vaccination rate of $\xi = 0.5\%$ per day (approximately seven months for the total population to be immunized), only if infection rate is kept near to the lower bound of ω . The

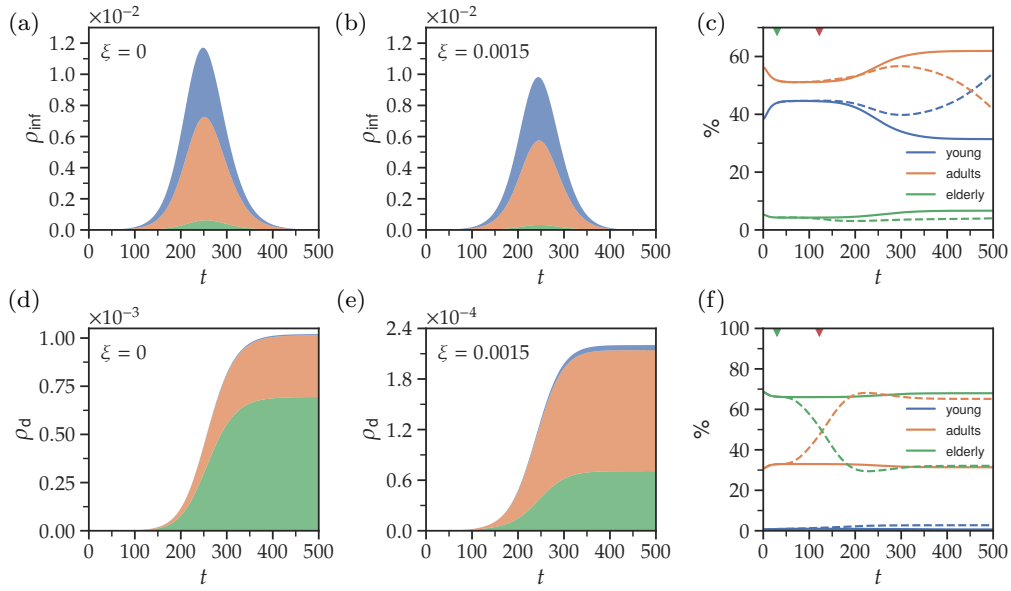


FIG. 6. Changes in the age profiles of infectious individuals and deaths with and without vaccination. Evolution of the fraction and age profiles of (a-c) infectious individuals and (d-e) accumulated deaths. The effects of DAP strategy with age-dependent values of efficacy against infection and death are addressed with a fixed vaccination rate $\xi = 0.15\%$ per day and delay of $t_v = 30$ days in a scenario of social distancing with $\omega = R_0^{\{S\}} = 1.3$. In the stack plots, the envelope gives the total prevalence or deaths while colors give the proportion within the young (0–19 yr, blue), adult (20–59 yr, orange), and elderly (≥ 60 yr, green) age groups. The age profiles for (c) infectious and (f) accumulated deaths give the percentage distribution for each group with (dashed lines) and without (solid lines) vaccination. Triangles indicate when the vaccinations of the elderly and adult populations start, while for the young population it has not started in the investigated time window. Note that the scales in (d) and (e) are different.

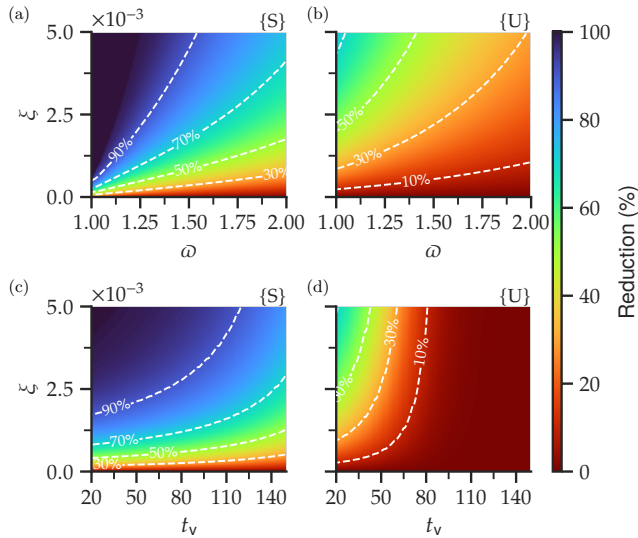


FIG. 7. Effects of infection rate and time delays for different vaccination rates in reducing the number of deaths. Heatmaps and isolines (white curves) for reduction of deaths using a DAP strategy and age-dependent values of efficacy against death and infection in comparison with the situation without vaccines. Fixed delay of $t_v = 30$ days is considered in (a,b) while a fixed infection rate given by $\omega = 1.3$ is considered in (c,d). Social distancing {S} and unmitigated {U} scenarios are presented in left and right-hand panels, respectively.

unmitigated scenario is not able to reduce the transmission by more than 10% in the whole parameter space, while we can still see a significant effect in the social distancing scenario; See Fig. SI-4 of the SM⁵⁵. The previous discussion was done for an early beginning of the vaccination. However, the intervention time t_v is a key parameter to the effectiveness of the vaccination. Heatmaps of death reduction in the ξ versus t_v space's parameter are presented in Fig. 7(c) and (d) for $\omega = 1.3$ ($R_0 > 1$ for $\xi = 0$ in both investigated scenarios). Delays are extremely harmful to the vaccination effectiveness even in the social distancing scenario shown in Fig. 7(c), in which one sees that the death reduction drops significantly for $t_v \gtrsim 80$ days, the more for lower vaccination rate. Delayed vaccination becomes ineffective in the scenarios without mitigation even at a high vaccination rate, as shown in Fig. 7(d).

B. Comparing strategies

Given the limited availability of vaccine shots, an essential problem is to determine which prioritization strategy can be more effective. Aiming at saving the maximum number of lives, we compared different strategies in the parameter space $\xi \times \omega$ shown in Fig. 8 for Brazilian demography (Fig. 2) and uniform values of vaccine efficacy against death and infection. To isolate the effects of different IFR age profiles (Fig. 4), the same epidemiological parameters of COVID-19, except the IFR itself, were considered. For the unreal case of age-

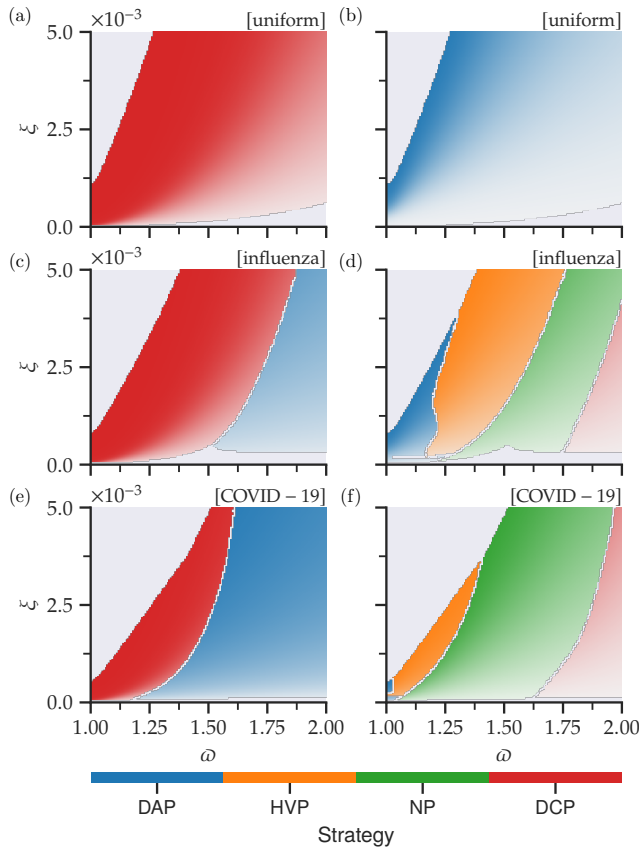


FIG. 8. Comparison of the most and least effective strategies for different IFR age profiles. The diagrams indicate the most (left) and least (right) effective strategies for reduction of deaths in the total population in the space parameter ξ versus ω . Three IFR age profiles are considered: (a,b) uniform, (c,d) influenza, and (e,f) COVID-19; See Fig. 4. Four vaccination strategies are considered: decreasing age (DAP), highly vulnerable (HVP), no (NP), and decreasing contact (DCP) priorities. A time delay of $t_v = 30$ days, vaccination with uniform values of efficacy against death and infection, Brazilian demography, and social distancing contact scenario were considered. The gradient colors refer to the respective reduction of deaths, the darker the higher. Differences between the most and least effective strategies smaller than 5% are depicted in gray.

independent IFR, the optimal strategy is to prioritize those who are more exposed, *i.e.* make more contacts, using DCP followed by no priority; the latter is better than the remaining ones since the adults constitute simultaneously the largest and most connected populations in Brazil. For influenza's IFR, we observe that prioritizing the most exposed individuals is more advantageous than the most vulnerable population for a broader region of the space parameter, especially if the vaccination rate is high. However, for uncontrolled transmission (high ω), it is still more effective to vaccinate according to a decreasing age criterion. Finally, the simulations with COVID-19's IFR yield that the most effective strategy is DAP in most of the investigated parameter space. Only in a narrow region, prioritizing the most exposed through DCP is the most effective. Notice that prioritizing only the highly vulnerable

(elderly) individuals by adopting the HVP strategy is not the most effective strategy in the investigated diagrams.

We also compute the least effective among the four investigated strategies, as shown in the right column of Fig. 8. For the uniform IFR age profile, the DAP strategy reduces deaths least while for realistic IFR of influenza and COVID-19, a complex pattern emerges in the diagrams. HVP can perform worst if the infection is moderately uncontrolled while DAP is the least effective only for almost controlled spreading ($\omega = R_0^{\{S\}} \approx 1$). A remarkable result is that prioritization of the most exposed is the least effective strategy if the epidemic is out of control. The respective plots for Uganda and Germany are shown in Fig. SI-5 of the SM⁵⁵.

The role of time delay in the strategy effectiveness is presented in Fig. 9 with fixed infection parameter $\omega = R_0^{\{S\}} = 1.3$ in a social distancing scenario, COVID-19's IFR age profile, and age-dependent values of efficiency. As shown in Fig. 9(a), DAP is the most effective for large delays while DCP is for earlier interventions. Moreover, the re-entrant behavior for intermediate delays ($t_v \sim 100$ days) reveals a complex interplay between epidemiological parameters and optimal strategies. No prioritization has the worst performance in almost the entire parameter diagram; See Fig. 9(b). Despite the unavoidable ethics concerns in prioritization strategies, a remarkable feature of these diagrams is that the optimal strategy depends, in a very nonlinear fashion, on the level of epidemic transmission, immunization rates, and timeliness of starting the vaccination.

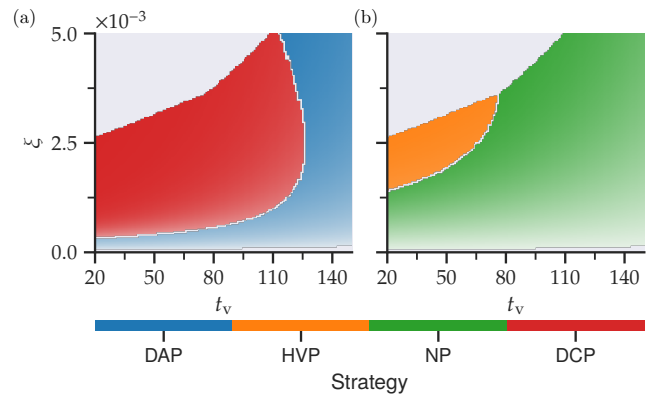


FIG. 9. Comparison of the most and least effective strategies considering different time delays. Diagrams indicating the (a) most and (b) least effective strategies to reduce deaths in the parameter space ξ versus t_v considering four strategies. The COVID-19' IFR age profile, contact scenario of social distancing, vaccination with age-dependent values of efficacy against death and infection, Brazilian demography, and infection rate given by and $\omega = 1.3$ were considered. Colors as in Fig. 8.

C. Effect of social contacts and demography

We have so far observed the nonlinear interplay between epidemiological parameters to determine the optimal strategy

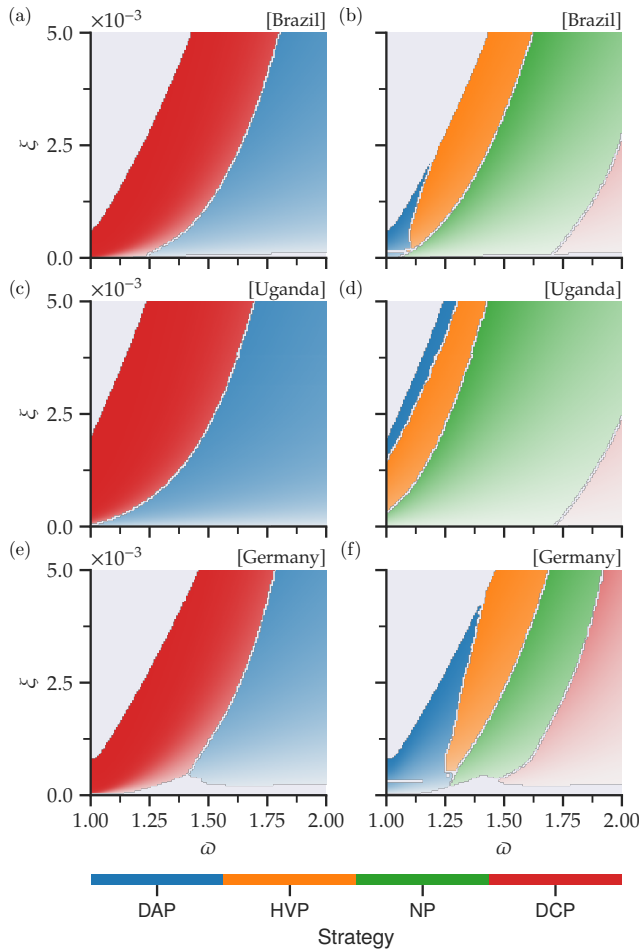


FIG. 10. Comparison of the most and least effective strategies for different demographic profiles. Diagrams indicating the optimal (left) and least effective (right) strategies in the parameter space ξ versus ω for (a,b) Brazil, (c,d) Uganda, and (e,f) Germany. The COVID-19's IFR age profile, a time delay of $t_v = 30$ days, vaccination with age-dependent values of efficacy against death and infection, and social distancing contact scenario were adopted. Colors as in Fig. 8.

to reduce deaths. It depends nontrivially on infection scenarios, vaccination rates, efficacy, and IFR age profiles. Now we explore the effect of demography and contact structures considering two other countries: Uganda, with a higher number of young individuals, and Germany, with a higher number of elderly individuals in comparison with Brazil. Table I summarizes the differences between young, adult and elderly populations in these countries while detailed demographics and contact patterns for Uganda and Germany are shown in Figs. SI-1 and SI-2 of the SM⁵⁵ in complement to Fig. 2 for Brazil.

Figure 10 presents the results of most and least effective strategies to reduce deaths considering age-dependent values of efficacy against death and infection and COVID-19's IFR age profile for Brazil, Uganda and Germany, while the results for uniform values of efficacy are shown in Figs. 8(e,f) and Fig. SI-5 of the SM⁵⁵. The plot for optimal strategies has the same qualitative patterns for the three countries with age

prioritization (DAP) being the most effective for higher infection regimes and contact prioritization (DCP) for lower infection and high vaccination rates. Quantitatively, Brazil and Germany present very similar diagrams despite the substantially higher fraction of elderly individuals in Germany. For Uganda, with a mostly young population, the diagram region where DAP outperforms DCP is larger than in Brazil and Germany. The last result seems counter-intuitive at a first glance since prioritizing the most exposed is expected to be more effective in a population with very few elderly (3.3%; See Table I). However, the most exposed population in Uganda are the young while in Germany and Brazil, adults perform more contacts; See Figs. 2, SI-1, and SI-2 of the SM⁵⁵. Since the COVID-19's IFR for the adult population is still much higher than for the young, DAP is also the best strategy for Uganda's contact pattern.

The least effective strategy provides more complex diagrams, depending strongly on the contact pattern and demography of the country. No priority strategy dominates the phase diagram for demographics of Brazil and Uganda. Prioritizing contacts is the least effective option for uncontrolled dissemination, more evidently for Germany's demography. Prioritizing age is the least effective option in a small region of the diagrams consisting of concomitantly low transmission and vaccination rate in the case of Brazil, with a broader region for Germany; See Figs. 10(b,f), respectively. The diagrams for optimal and least effective strategies for young, adults, and elderly individuals also present nonlinear effects. Moreover, the diagrams for the whole population are ruled by deaths of elderly; See Figs. SI-6 and SI-7 of the SM⁵⁵.

IV. CONCLUSION

The rise of a new, highly transmissible, and lethal infectious disease implies an enormous logistic challenge to minimize the damages and, especially in the case of viral pathogens, quick development and massive distribution of vaccines to the entire population is the most, maybe the only, viable option to mitigate the impacts of the disease. Moreover, the capability of the viruses in mutating and thus evading the protection conferred by either previous infections or vaccination imposes a constant concern about the optimal prioritization strategy to be adopted in a realistic scenario of a limited supply of vaccine shots. We are nowadays witnessing a remarkable success of massive vaccination to reduce the severe cases of COVID-19, wherever it has been adopted.

The choice of the optimal prioritization strategy aiming at reducing the number of severe cases and consequently of deaths is far from being trivial due to the wide pool of relevant epidemiological parameters involved in the analysis. Healthcare authorities should be aware that there is not a unique optimal strategy that performs better in all situations due to the nonlinear complexity of the subject. To contribute to this problem, we investigated the role of social contact patterns (Fig. 2) and infection fatality ratio (Fig. 4) on vaccine prioritization strategies using an age-structured compartmental model and a data-driven approach, in which real epidemio-

logical parameters are used as inputs to the numerical analysis. Prioritization of the most vulnerable population (with high risk of death) and of the most exposed individuals (who perform more contacts) were compared with no prioritization. We report that vaccines, even with modest protection against infections, are very effective to reduce fatality irrespective of the strategy. For age prioritization, which corresponds to the most vulnerable population in several infectious diseases and particularly in COVID-19, the age profiles of deaths are significantly altered while the infection profile changes comparatively little. Another important outcome of the simulations is that the effectiveness of the vaccination depends strongly on the contagion mitigation. Delays in starting vaccination imply the ineffectiveness of vaccines if the contagion is uncontrolled.

The optimal and least effective strategy to reduce deaths also depends on the epidemic scenario and IFR age profile. Vaccination of the most exposed population first is more effective than of the most vulnerable individuals when the epidemic is highly controlled with a low transmission rate. The prioritization of the most vulnerable population becomes the optimal approach for highly contagious scenarios. However, nonlinear dependence on the vaccination and contagion rates, depending on the IFR profile, is observed. Comparing COVID-19 and seasonal influenza IFRs, we report that the region in the epidemiological parameter space, where prioritizing vulnerable persons is the most effective strategy, is broader for the former, despite the qualitative similarity between them. This is in agreement with other results in the literature, such as the adoption of a DAP-like strategy for COVID-19^{23–25,31}, and a mix of DAP-like and DCP-like strategies for influenza^{24,54}. It is also important to notice the differences between Fig. 8(e), for a vaccine with uniform protection across different age groups, and Fig. 10(a), considering age-dependent values of efficacy. The region in which the DCP outperforms DAP strategy is larger in the latter, for which the effectiveness of the vaccine for elderly individuals is assumed to be lower and blocking the transmission is more efficient. Finally, the diagrams in the epidemiological space parameter reporting the optimal strategy depend little on demography and social contact profile when comparing data for Brazil, Germany, and Uganda, which present very distinct patterns. However, the least effective strategy is very sensitive to demography and contact matrices, revealing a complex dependence on epidemiological parameters.

The data-driven analysis developed in this work raises important issues, from the perspective of nonlinear dynamical systems, that may be underestimated in applied mathematical or statistical epidemiological modeling. This kind of modeling can help decision-makers to select the vaccination prioritization strategy according to the current scenario, but our central aim is to quantitatively address the importance of epidemiological parameters on the outcomes of the theoretical analysis using a mechanistic approach. Some simple, but still essential messages were presented. Beyond the obvious ones reporting that the faster and earlier the vaccination, the better its result is, we also show that the outcomes depend nonlinearly on the epidemiological situation and particularities of

the infectious disease. We expect that our more mechanistic approach can join statistical inference methods to provide more accurate responses to vaccination prioritization strategies.

SUPPLEMENTARY MATERIAL

See [supplementary material](#) for demography and contact structure of Uganda and Germany, impact of DAP vaccination for uniform values of efficacy, reduction of recovered individuals with age-dependent values of efficacy, optimal and least effective strategies for Uganda and Germany contact patterns, and optimal and least effective strategies for young, adult and elderly populations.

ACKNOWLEDGMENTS

A.S., W.C., and S.C.F. acknowledge financial support from Coordenação de Aperfeiçoamento de Pessoal de Nível Superior – CAPES <https://www.gov.br/capes/> (grant No. 88887.507046/2020-00). S.C.F. acknowledge financial support from Conselho Nacional de Desenvolvimento Científico e Tecnológico – CNPq <https://www.gov.br/cnpq/> (grants No. 430768/2018-4 and 311183/2019-0) and Fundação de Amparo à Pesquisa do Estado de Minas Gerais – FAPEMIG <https://fapemig.br/> (grant No. APQ-02393-18). This study was financed in part by Coordenação de Aperfeiçoamento de Pessoal de Nível Superior – CAPES - Finance Code 001. The funders had no role in study design, data collection and analysis, decision to publish, or preparation of the manuscript.

DATA AVAILABILITY

The data that support the findings of this study are openly available in the Github repository at <https://github.com/wcota/covid19-vac-st/>.

CONFLICT OF INTEREST

The authors have no conflicts to disclose.

AUTHORS CONTRIBUTIONS

Conceptualization, Supervision, Project Administration, and Original Draft Preparation: Wesley Cota, Silvio C. Ferreira; **Data Curation and Software:** Arthur Schulenburg, Wesley Cota; **Visualization:** Wesley Cota; **Funding Acquisition:** Silvio C. Ferreira; **Formal Analysis, Investigation, Methodology, Validation, and Review & Editing:** Arthur Schulenburg, Wesley Cota, Guilherme S. Costa, Silvio C. Ferreira.

- ¹S. Moore, E. M. Hill, M. J. Tildesley, L. Dyson, and M. J. Keeling, “Vaccination and non-pharmaceutical interventions for COVID-19: a mathematical modelling study,” *Lancet Infect. Dis.* **21**, 793–802 (2021).
- ²C. J. Worry and H.-H. Chang, “Face mask use in the general population and optimal resource allocation during the COVID-19 pandemic,” *Nat. Commun.* **11**, 4049 (2020).
- ³P. C. Ventura, A. Aleta, F. A. Rodrigues, and Y. Moreno, “Modeling the effects of social distancing on the large-scale spreading of diseases,” *Epidemics* **38**, 100544 (2022).
- ⁴S. Pei, S. Kandula, and J. Shaman, “Differential effects of intervention timing on COVID-19 spread in the United States,” *Sci. Adv.* **6**, eabd6370 (2020).
- ⁵Y. Bo, C. Guo, C. Lin, Y. Zeng, H. B. Li, Y. Zhang, M. S. Hossain, J. W. Chan, D. W. Yeung, K. O. Kwok, S. Y. Wong, A. K. Lau, and X. Q. Lao, “Effectiveness of non-pharmaceutical interventions on COVID-19 transmission in 190 countries from 23 January to 13 April 2020,” *Int. J. Infect. Dis.* **102**, 247–253 (2021).
- ⁶R. Vardavas, A. Strong, J. Bouey, J. Welburn, P. de Lima, L. Baker, K. Zhu, M. Priest, L. Hu, and J. Ringel, *The Health and Economic Impacts of Non-pharmaceutical Interventions to Address COVID-19: A Decision Support Tool for State and Local Policymakers* (RAND Corporation, 2020).
- ⁷T. Alpert, A. F. Brito, E. Lasek-Nesselquist, J. Rothman, A. L. Valesano, M. J. MacKay, M. E. Petrone, M. I. Breban, A. E. Watkins, C. B. Vogels, C. C. Kalinich, S. Dellicour, A. Russell, J. P. Kelly, M. Shudt, J. Plitnick, E. Schneider, W. J. Fitzsimmons, G. Khullar, J. Metti, J. T. Dudley, M. Nash, N. Beaubier, J. Wang, C. Liu, P. Hui, A. Muyombwe, R. Downing, J. Razeq, S. M. Bart, A. Grills, S. M. Morrison, S. Murphy, C. Neal, E. Laszlo, H. Rennert, M. Cushing, L. Westblade, P. Velu, A. Craney, L. Cong, D. R. Peaper, M. L. Landry, P. W. Cook, J. R. Fauver, C. E. Mason, A. S. Lauring, K. S. George, D. R. MacCannell, and N. D. Grubaugh, “Early introductions and transmission of SARS-CoV-2 variant B.1.1.7 in the United States,” *Cell* **184**, 2595–2604.e13 (2021).
- ⁸M. Alene, L. Yismaw, M. A. Assemie, D. B. Ketema, W. Gietaneh, and T. Y. Birhan, “Serial interval and incubation period of COVID-19: a systematic review and meta-analysis,” *BMC Infect. Dis.* **21**, 257 (2021).
- ⁹D. Planas, T. Bruel, L. Grzelak, F. Guivel-Benhassine, I. Staropoli, F. Porrot, C. Planchais, J. Buchrieser, M. M. Rajah, E. Bishop, M. Albert, F. Donati, M. Prot, S. Behillil, V. Enouf, M. Maquart, M. Smati-Lafarge, E. Varon, F. Schortgen, L. Yahyaoui, M. Gonzalez, J. D. Sèze, H. Péré, D. Veyer, A. Sève, E. Simon-Lorière, S. Fafi-Kremer, K. Stefic, H. Mouquet, L. Hocqueloux, S. van der Werf, T. Prazuck, and O. Schwartz, “Sensitivity of infectious SARS-CoV-2 B.1.1.7 and B.1.351 variants to neutralizing antibodies,” *Nat. Med.* **27**, 917–924 (2021).
- ¹⁰F. G. Naveca, V. Nascimento, V. C. de Souza, A. de Lima Corado, F. Nascimento, G. Silva, Á. Costa, D. Duarte, K. Pessoa, M. Mejía, M. J. Brandão, M. Jesus, L. Gonçalves, C. F. da Costa, V. Sampaio, D. Barros, M. Silva, T. Mattos, G. Pontes, L. Abdalla, J. H. Santos, I. Arantes, F. Z. Dezordi, M. M. Siqueira, G. L. Wallau, P. C. Resende, E. Delatorre, T. Gräf, and G. Bello, “COVID-19 in Amazonas, Brazil, was driven by the persistence of endemic lineages and P.1 emergence,” *Nat. Med.* **27**, 1230–1238 (2021).
- ¹¹W. Zhou and W. Wang, “Fast-spreading SARS-CoV-2 variants: challenges to and new design strategies of COVID-19 vaccines,” *Signal Transduct. Target. Ther.* **6**, 226 (2021).
- ¹²F. Campbell, B. Archer, H. Laurenson-Schafer, Y. Jinnai, F. Konings, N. Batra, B. Pavlin, K. Vandemaele, M. D. V. Kerkhove, T. Jombart, O. Morgan, and O. le Polain de Waroux, “Increased transmissibility and global spread of SARS-CoV-2 variants of concern as at June 2021,” *Eurosurveillance* **26**, 2100509 (2021).
- ¹³K. Kupferschmidt and M. Wadman, “Delta variant triggers new phase in the pandemic,” *Science* **372**, 1375–1376 (2021).
- ¹⁴P. R. Matt J. Keeling, *Modeling Infectious Diseases in Humans and Animals* (PRINCETON UNIV PR, 2007).
- ¹⁵D. Sridhar and D. Gurdasani, “Herd immunity by infection is not an option,” *Science* **371**, 230–231 (2021).
- ¹⁶P. M. Heaton, “The Covid-19 vaccine-development multiverse,” *N. Engl. J. Med.* **383**, 1986–1988 (2020).
- ¹⁷P. Ball, “The lightning-fast quest for COVID vaccines — and what it means for other diseases,” *Nature* **589**, 16–18 (2020).
- ¹⁸R. Palacios, A. P. Batista, C. S. N. Albuquerque, E. G. Patiño, J. do Prado Santos, M. T. R. P. Conde, R. de Oliveira Piorelli, L. C. P. Júnior, S. M. Raboni, F. Ramos, G. A. S. Romero, F. E. Leal, L. F. A. Camargo, F. H. Aoki, E. B. Coelho, D. S. Oliveira, C. J. F. Fontes, G. C. S. Pileggi, A. L. L. de Oliveira, A. M. de Siqueira, D. B. L. de Oliveira, V. F. Boto-sso, G. Zeng, Q. Xin, M. M. Teixeira, M. L. Nogueira, and E. G. Kallas, “Efficacy and safety of a COVID-19 inactivated vaccine in healthcare professionals in Brazil: The PROFISCOV study,” *SSRN Electronic Journal* (2021), 10.2139/ssrn.3822780.
- ¹⁹I. Yelin, R. Katz, E. Herzl, T. Berman-Zilberstein, A. Ben-Tov, J. Kuint, S. Gazit, T. Patalon, G. Chodick, and R. Kishony, “Associations of the BNT162b2 COVID-19 vaccine effectiveness with patient age and comorbidities,” *MedRxiv* (2021), 10.1101/2021.03.16.21253686.
- ²⁰A. Jara, E. A. Undurraga, C. González, F. Paredes, T. Fontecilla, G. Jara, A. Pizarro, J. Acevedo, K. Leo, F. Leon, C. Sans, P. Leighton, P. Suárez, H. García-Escorza, and R. Araos, “Effectiveness of an inactivated SARS-CoV-2 vaccine in Chile,” *N. Engl. J. Med.* (2021), 10.1056/nejmoa2107715.
- ²¹O. T. Ranzani, M. D. T. Hitchings, M. Dorion, T. L. D’Agostini, R. C. de Paula, O. F. P. de Paula, E. F. d. M. Villela, M. S. S. Torres, S. B. de Oliveira, W. Schulz, M. Almiron, R. Said, R. D. de Oliveira, P. Vieira da Silva, W. N. de Araújo, J. C. Gorinchteyn, J. R. Andrews, D. A. T. Cummings, A. I. Ko, and J. Croda, “Effectiveness of the CoronaVac vaccine in older adults during a gamma variant associated epidemic of covid-19 in Brazil: test negative case-control study,” *BMJ* **374**, n2015 (2021).
- ²²R. W. Frenck, N. P. Klein, N. Kitchin, A. Gurtman, J. Absalon, S. Lockhart, J. L. Perez, E. B. Walter, S. Senders, R. Bailey, K. A. Swanson, H. Ma, X. Xu, K. Koury, W. V. Kalina, D. Cooper, T. Jennings, D. M. Brandon, S. J. Thomas, Özlem Türeci, D. B. Tresnan, S. Mather, P. R. Dormitzer, U. Şahin, K. U. Jansen, and W. C. Gruber, “Safety, immunogenicity, and efficacy of the BNT162b2 Covid-19 vaccine in adolescents,” *N. Engl. J. Med.* **385**, 239–250 (2021).
- ²³J. R. Goldstein, T. Cassidy, and K. W. Wachter, “Vaccinating the oldest against COVID-19 saves both the most lives and most years of life,” *PNAS* **118**, e2026322118 (2021).
- ²⁴M. C. Fitzpatrick and A. P. Galvani, “Optimizing age-specific vaccination,” *Science* **371**, 890–891 (2021).
- ²⁵L. Matrajt, J. Eaton, T. Leung, and E. R. Brown, “Vaccine optimization for COVID-19: Who to vaccinate first?” *Sci. Adv.* **7**, eabf1374 (2020).
- ²⁶M. Moret, T. R. Filho, J. Mendes, T. Murari, A. N. Filho, A. Cordeiro, W. Ramalho, F. Scorza, and A.-C. Almeida, “WHO vaccination protocol can be improved to save more lives,” *Res. Sq.* (2021), 10.21203/rs.3.rs-148826/v1.
- ²⁷L. Matrajt, J. Eaton, T. Leung, D. Dimitrov, J. T. Schiffer, D. A. Swan, and H. Janes, “Optimizing vaccine allocation for COVID-19 vaccines shows the potential role of single-dose vaccination,” *Nat. Commun.* **12**, 3449 (2021).
- ²⁸S. L. Li, R. H. M. Pereira, C. A. P. Jr, A. E. Zarebski, L. Emanuel, P. J. H. Alves, P. S. Peixoto, C. K. V. Braga, A. A. de Souza Santos, W. M. de Souza, R. J. Barbosa, L. F. Buss, A. Mendrone, C. de Almeida-Neto, S. C. Ferreira, N. A. Salles, I. Marcilio, C.-H. Wu, N. Gouveia, V. H. Nascimento, E. C. Sabino, N. R. Faria, and J. P. Messina, “Higher risk of death from COVID-19 in low-income and non-white populations of São Paulo, Brazil,” *BMJ Glob. Health* **6**, e004959 (2021).
- ²⁹E. J. Emanuel, G. Persad, A. Kern, A. Buchanan, C. Fabre, D. Halliday, J. Heath, L. Herzog, R. J. Leland, E. T. Lemango, F. Luna, M. S. McCoy, O. F. Norheim, T. Ottersen, G. O. Schaefer, K.-C. Tan, C. H. Wellman, J. Wolff, and H. S. Richardson, “An ethical framework for global vaccine allocation,” *Science* **369**, 1309–1312 (2020).
- ³⁰C. Buckee, A. Noor, and L. Sattenspiel, “Thinking clearly about social aspects of infectious disease transmission,” *Nature* **595**, 205–213 (2021).
- ³¹M. C. Castro and B. Singer, “Prioritizing COVID-19 vaccination by age,” *PNAS* **118**, e2103700118 (2021).
- ³²G. Giordano, M. Colaneri, A. D. Filippo, F. Blanchini, P. Bolzern, G. D. Nicolao, P. Sacchi, P. Colaneri, and R. Bruno, “Modeling vaccination roll-outs, SARS-CoV-2 variants and the requirement for non-pharmaceutical interventions in Italy,” *Nat. Med.* **27**, 993–998 (2021).
- ³³K. M. Bubar, K. Reinholt, S. M. Kissler, M. Lipsitch, S. Cobey, Y. H. Grad, and D. B. Larremore, “Model-informed COVID-19 vaccine prioritization strategies by age and serostatus,” *Science* **371**, 916–921 (2021).
- ³⁴J. H. Buckner, G. Chowell, and M. R. Springborn, “Optimal dynamic prioritization of scarce COVID-19 vaccines,” *MedRxiv* (2020), 10.1101/2020.09.22.20199174.

- ³⁵J. Molla, A. P. de León Chávez, T. Hiraoka, T. Ala-Nissila, M. Kivela, and L. Leskelä, “Adaptive and optimized COVID-19 vaccination strategies across geographical regions and age groups,” *PLOS Comput. Biol.* **18**, e1009974 (2022).
- ³⁶O. Milman, I. Yelin, N. Aharoni, R. Katz, E. Herzel, A. Ben-Tov, J. Kuint, S. Gazit, G. Chodick, T. Patalon, and R. Kishony, “Community-level evidence for SARS-CoV-2 vaccine protection of unvaccinated individuals,” *Nat. Med.* **27**, 1367–1369 (2021).
- ³⁷R. Pastor-Barriuso, B. Pérez-Gómez, M. A. Hernán, M. Pérez-Olmeda, R. Yotti, J. Oteo-Iglesias, J. L. Sanmartín, I. León-Gómez, A. Fernández-García, P. Fernández-Navarro, I. Cruz, M. Martín, C. Delgado-Sanz, N. F. de Larrea, J. L. Paniagua, J. F. Muñoz-Montalvo, F. Blanco, A. Larrauri, and M. Pollán, “Infection fatality risk for SARS-CoV-2 in community dwelling population of Spain: nationwide seroepidemiological study,” *BMJ* **371**, m4509 (2020).
- ³⁸J. P. A. Ioannidis, “Infection fatality rate of COVID-19 inferred from seroprevalence data,” *Bull. World Health Organ.* **99**, 19–33F (2020).
- ³⁹S. Mallapaty, “How deadly is the coronavirus? scientists are close to an answer,” *Nature* **582**, 467–468 (2020).
- ⁴⁰I. R. Barbosa, M. H. R. Galvão, T. A. de Souza, S. M. Gomes, A. de Almeida Medeiros, and K. C. de Lima, “Incidence of and mortality from COVID-19 in the older Brazilian population and its relationship with contextual indicators: an ecological study,” *Rev. Bras. Geriatr. Gerontol.* **23**, e200171 (2020).
- ⁴¹M. C. Castro, S. Gurzenda, E. M. Macário, and G. V. A. França, “Characteristics, outcomes and risk factors for mortality of 522 167 patients hospitalised with COVID-19 in Brazil: a retrospective cohort study,” *BMJ Open* **11**, e049089 (2021).
- ⁴²P. Poletti, M. Tirani, D. Cereda, F. Trentini, G. Guzzetta, V. Marziano, S. Buoro, S. Riboli, L. Crotogini, R. Piccarreta, A. Piatti, G. Grasselli, A. Melegaro, M. Gramegna, M. Ajelli, and S. Merler, “Age-specific SARS-CoV-2 infection fatality ratio and associated risk factors, Italy, February to April 2020,” *Eurosurveillance* **25**, 2001383 (2020).
- ⁴³A. T. Levin, W. P. Hanage, N. Owusu-Boaitey, K. B. Cochran, S. P. Walsh, and G. Meyerowitz-Katz, “Assessing the age specificity of infection fatality rates for COVID-19: systematic review, meta-analysis, and public policy implications,” *Eur. J. Epidemiol.* **35**, 1123–1138 (2020).
- ⁴⁴R. Verity, L. C. Okell, I. Dorigatti, P. Winskill, C. Whittaker, N. Imai, G. Cuomo-Dannenburg, H. Thompson, P. G. T. Walker, H. Fu, A. Dighe, J. T. Griffin, M. Baguelin, S. Bhatia, A. Boonyasiri, A. Cori, Z. Cucunubá, R. FitzJohn, K. Gaythorpe, W. Green, A. Hamlet, W. Hinsley, D. Laydon, G. Nedjati-Gilani, S. Riley, S. van Elsland, E. Volz, H. Wang, Y. Wang, X. Xi, C. A. Donnelly, A. C. Ghani, and N. M. Ferguson, “Estimates of the severity of coronavirus disease 2019: a model-based analysis,” *Lancet Infect. Dis.* **20**, 669–677 (2020).
- ⁴⁵Centers for Disease Control and Prevention, “Estimated influenza illnesses, medical visits, hospitalizations, and deaths in the United States—2018–2019 influenza season,” <https://www.cdc.gov/fl/about/burden-averted/2019-2020.htm> (2020).
- ⁴⁶N. G. Davies, P. Klepac, Y. Liu, K. Prem, M. Jit, C. A. B. Pearson, B. J. Quilty, A. J. Kucharski, H. Gibbs, S. Clifford, A. Gimma, K. van Zandvoort, J. D. Munday, C. Diamond, W. J. Edmunds, R. M. G. J. Houben, J. Hellewell, T. W. Russell, S. Abbott, S. Funk, N. I. Bosse, Y. F. Sun, S. Flasche, A. Rosello, C. I. Jarvis, and R. M. E. and, “Age-dependent effects in the transmission and control of COVID-19 epidemics,” *Nat. Med.* **26**, 1205–1211 (2020).
- ⁴⁷K. E. Johnson, M. Lachmann, M. Stoddard, R. Pasco, S. J. Fox, L. A. Meyers, and A. Chakravarty, “Detecting in-school transmission of SARS-CoV-2 from case ratios and documented clusters,” *MedRxiv* (2021), 10.1101/2021.04.26.21256136.
- ⁴⁸M. Cevik and S. D. Baral, “Networks of SARS-CoV-2 transmission,” *Science* **373**, 162–163 (2021).
- ⁴⁹J. M. Epstein, E. Hatna, and J. Crodelle, “Triple contagion: a two-fears epidemic model,” *J. R. Soc. Interface* **18**, 20210186 (2021).
- ⁵⁰K. Prem, A. R. Cook, and M. Jit, “Projecting social contact matrices in 152 countries using contact surveys and demographic data,” *PLOS Comput. Biol.* **13**, e1005697 (2017).
- ⁵¹Z. Wang, C. T. Bauch, S. Bhattacharyya, A. d’Onofrio, P. Manfredi, M. Perc, N. Perra, M. Salathé, and D. Zhao, “Statistical physics of vaccination,” *Phys. Rep.* **664**, 1–113 (2016).
- ⁵²Instituto Brasileiro de Geografia e Estatística, ed., *Projeções da população: Brasil e unidades da Federação, revisão 2018*, 2nd ed., Séries Relatórios metodológicos No. volume 40 (IBGE, Instituto Brasileiro de Geografia e Estatística, Rio de Janeiro, 2018).
- ⁵³United Nations, “World Population Prospects 2019,” Department of Economic and Social Affairs, Population Division (2019).
- ⁵⁴J. Medlock and A. P. Galvani, “Optimizing influenza vaccine distribution,” *Science* **325**, 1705–1708 (2009).
- ⁵⁵Supplementary Material.
- ⁵⁶Q. Li, X. Guan, P. Wu, X. Wang, L. Zhou, Y. Tong, R. Ren, K. S. Leung, E. H. Lau, J. Y. Wong, X. Xing, N. Xiang, Y. Wu, C. Li, Q. Chen, D. Li, T. Liu, J. Zhao, M. Liu, W. Tu, C. Chen, L. Jin, R. Yang, Q. Wang, S. Zhou, R. Wang, H. Liu, Y. Luo, Y. Liu, G. Shao, H. Li, Z. Tao, Y. Yang, Z. Deng, B. Liu, Z. Ma, Y. Zhang, G. Shi, T. T. Lam, J. T. Wu, G. F. Gao, B. J. Cowling, B. Yang, G. M. Leung, and Z. Feng, “Early transmission dynamics in Wuhan, China, of novel coronavirus-infected pneumonia,” *N. Engl. J. Med.* **382**, 1199–1207 (2020).
- ⁵⁷S. Zhang, M. Diao, W. Yu, L. Pei, Z. Lin, and D. Chen, “Estimation of the reproductive number of novel coronavirus (COVID-19) and the probable outbreak size on the diamond princess cruise ship: A data-driven analysis,” *Int. J. Infect. Dis.* **93**, 201–204 (2020).
- ⁵⁸R. Li, S. Pei, B. Chen, Y. Song, T. Zhang, W. Yang, and J. Shaman, “Substantial undocumented infection facilitates the rapid dissemination of novel coronavirus (SARS-CoV-2),” *Science* **368**, 489–493 (2020).
- ⁵⁹S. Sanche, Y. T. Lin, C. Xu, E. Romero-Severson, N. Hengartner, and R. Ke, “High contagiousness and rapid spread of severe acute respiratory syndrome coronavirus 2,” *Emerging Infect. Dis.* **26**, 1470–1477 (2020).
- ⁶⁰T. Cerqueira-Silva, V. de Araújo Oliveira, V. S. Boaventura, J. M. Pescarini, J. B. Júnior, T. M. Machado, R. Flores-Ortiz, G. O. Penna, M. Y. Ichihara, J. V. de Barros, M. L. Barreto, G. L. Werneck, and M. Barral-Netto, “Influence of age on the effectiveness and duration of protection of Vaxzevria and CoronaVac vaccines: A population-based study,” *The Lancet Regional Health - Americas* **6**, 100154 (2022).
- ⁶¹M. Levine-Tiefenbrun, I. Yelin, R. Katz, E. Herzel, Z. Golan, L. Schreiber, T. Wolf, V. Nadler, A. Ben-Tov, J. Kuint, S. Gazit, T. Patalon, G. Chodick, and R. Kishony, “Initial report of decreased SARS-CoV-2 viral load after inoculation with the BNT162b2 vaccine,” *Nat. Med.* **27**, 790–792 (2021).
- ⁶²J. M. Read, J. R. E. Bridgen, D. A. T. Cummings, A. Ho, and C. P. Jewell, “Novel coronavirus 2019-nCoV (COVID-19): early estimation of epidemiological parameters and epidemic size estimates,” *Philos. Trans. R. Soc. Lond., B, Biol. Sci.* **376**, 20200265 (2021).
- ⁶³L. Danon, E. Brooks-Pollock, M. Bailey, and M. Keeling, “A spatial model of COVID-19 transmission in England and Wales: early spread, peak timing and the impact of seasonality,” *Philos. Trans. R. Soc. Lond., B, Biol. Sci.* **376**, 20200272 (2021).
- ⁶⁴G. Chodick, L. Tene, T. Patalon, S. Gazit, A. B. Tov, D. Cohen, and K. Muhsen, “Assessment of effectiveness of 1 dose of BNT162b2 vaccine for SARS-CoV-2 infection 13 to 24 days after immunization,” *JAMA Network Open* **4**, e2115985 (2021).
- ⁶⁵B. F. Maier, A. Burdinski, A. H. Rose, F. Schlosser, D. Hinrichs, C. Betsch, L. Korn, P. Sprengholz, M. Meyer-Hermann, T. Mitra, K. Lauterbach, and D. Brockmann, “Potential benefits of delaying the second mRNA COVID-19 vaccine dose,” *ArXiv* (2021), arXiv:2102.13600 [q-bio.PE].